
Feasibility of Dual-Isotope Coincidence/Single-Photon Imaging of the Myocardium

Edward V.R. Di Bella, Dan J. Kadrmaz, and Paul E. Christian

Medical Imaging Research Laboratory, Department of Radiology, University of Utah, Salt Lake City, Utah

Hybrid PET scanners offer the possibility of obtaining myocardial viability information from coincidence imaging of the positron emitter ^{18}F -FDG and perfusion measurements from a single-photon tracer—potentially simultaneously. This new approach is less costly and more readily available than dedicated PET and offers potential for improved FDG resolution and sensitivity compared with SPECT with 511-keV collimators. Simultaneous imaging of the coincidence and single-photon events offers the further advantages of automatic image registration and reduced imaging time. However, the feasibility of simultaneous coincidence/single-photon imaging or even immediately sequential imaging is unknown. In this study, the potential of using standard low-energy high-resolution (LEHR) collimators with hybrid PET to obtain coincidence and SPECT data was assessed. **Methods:** Phantom and human studies were performed to investigate the effect of LEHR collimators on FDG coincidence imaging with a hybrid PET system, the effect of the presence of $^{99\text{m}}\text{Tc}$ during FDG coincidence imaging with LEHR collimators, and the effect of the presence of FDG during $^{99\text{m}}\text{Tc}$ SPECT imaging. **Results:** FDG images were somewhat degraded (a measure of myocardial nonuniformity increased 10%) with LEHR collimators. With 148 MBq (4 mCi) $^{99\text{m}}\text{Tc}$ present during FDG imaging of a phantom, image quality was maintained and the number of detected coincidences changed by <5%. With $^{99\text{m}}\text{Tc}/^{18}\text{F}$ whole-body ratios of 7:1, crosstalk from ^{18}F photons accounted for the majority of counts in the $^{99\text{m}}\text{Tc}$ SPECT images and resulted in severe artifacts. The artifacts were decreased with a simple crosstalk correction scheme but remained problematic. **Conclusion:** $^{99\text{m}}\text{Tc}/^{18}\text{F}$ ratios of at least 9:1 and state-of-the-art reconstruction and crosstalk correction are likely to be required to perform immediately sequential coincidence/single-photon imaging of the myocardium with clinically useful results. Additional challenges remain before simultaneous imaging of coincidence events and single photons can be realized in practice.

Key Words: hybrid PET; SPECT; dual isotope; cardiac imaging
J Nucl Med 2001; 42:944–950

Determination of myocardial perfusion and viability is important for diagnosing and ascertaining the prognosis of coronary artery disease. Relative myocardial perfusion can

be measured with a variety of $^{99\text{m}}\text{Tc}$ -labeled or ^{201}Tl single-photon emitters or with positron emitters. For the noninvasive assessment of myocardial viability, PET imaging of ^{18}F -FDG is the current gold standard. FDG SPECT with 511-keV collimators has been shown to provide a clinically useful assessment of viability, though generally not equivalent to that provided by FDG PET (1,2). Compared with SPECT with 511-keV collimators, the new hybrid PET camera systems may offer benefits for cardiac viability imaging; coincidence detection provides better resolution and lacks the mammoth lead collimators that block most of the incident photons. Recently, some publications relevant to cardiac imaging with hybrid PET systems have appeared (3–5), although the lack of built-in attenuation correction methods has made cardiac imaging with hybrid PET impractical. This situation has changed lately, with several manufacturers now offering solutions.

Simultaneous measurement of myocardial perfusion and viability has several advantages over separate acquisitions, including intrinsic registration of the datasets, decreased motion artifacts, and increased throughput. For the case of SPECT with 511-keV collimators, energy discrimination permits the simultaneous imaging of FDG and a $^{99\text{m}}\text{Tc}$ -tagged pharmaceutical, although both agents are imaged with the 511-keV collimator. Such simultaneous viability and perfusion measurements using SPECT have been reported (6–8). A good review of FDG imaging with SPECT, including dual-isotope FDG/ $^{99\text{m}}\text{Tc}$ -sestamibi acquisitions, has been given by Sandler et al. (3,9).

Using coincidence-capable gamma cameras in fully 3-dimensional mode with low-energy high-resolution (LEHR) collimators mounted may enable simultaneous perfusion/viability imaging with improved resolution and a lowered dose of positron emitter, compared with 511-keV collimated imaging (10). Because the LEHR collimators are easily penetrated by the 511-keV photons, coincidence imaging is similar to imaging with “open-frame” collimators. However, several problems arise from the hybrid PET approach to simultaneous perfusion/viability imaging. One problem is that axial slat collimators cannot be used in conjunction with LEHR collimators. Axial slat collimators are narrow slats of lead septa running perpendicular to the z-axis of the scanner. The lead slats block interslice coincidences. Although some type of hybrid LEHR/lead slat col-

Received Aug. 7, 2000; revision accepted Feb. 14, 2001.
For correspondence or reprints contact: Edward V.R. Di Bella, PhD, MIRL/Radiology, 729 Arapsee Dr., Salt Lake City, UT 84108.

limator could be designed, the slats would block a significant portion of the low-energy data. Another potential problem is the impact of the presence of ^{99m}Tc on ^{18}F imaging in terms of increasing dead time. And the final serious problem is the crosstalk from 511-keV photons scattering or depositing a fraction of their energy in the crystal and masquerading as ^{99m}Tc photons.

The goal of this study was to evaluate the feasibility of using a hybrid PET system to image FDG with LEHR collimators in place and ^{99m}Tc present and immediately thereafter acquiring ^{99m}Tc SPECT data. If such an approach to cardiac imaging is feasible, truly simultaneous acquisitions are then possible, although additional hardware may be necessary to minimize imaging time.

MATERIALS AND METHODS

The Effect of LEHR Collimators on Coincidence Imaging

Phantom Study. A cardiac thorax phantom (Data Spectrum Corp., Hillsborough, NC) was filled with water, and a transmission scan using 2 scanning ^{133}Ba point sources (365 keV) was obtained. ^{18}F was added to give 10 MBq (0.27 mCi) in the myocardial insert (93.5 kBq/mL), 9.6 MBq (0.26 mCi) ^{18}F in the liver (7.8 kBq/mL), and 37 MBq (1.0 mCi) ^{18}F in the background (4.2 kBq/mL). The phantom was imaged with an IRIX hybrid PET scanner (Marconi Medical Systems, Cleveland, OH) with 2 coincidence detectors and used 60 gantry angles over 180° , with 20 s at each angle. Axial slat collimators were used. The axial slat collimators were then replaced with standard LEHR collimators (2.7 cm thick, 0.12-cm hole size), and 1 h later the coincidence acquisition was repeated with the phantom in the same position on the bed. The second acquisition used 60 gantry angles, with 30 s at each angle. At each gantry stop, list-mode coincidence data were acquired over a range of approximately $\pm 20^\circ$ (this is a function of the radius of the camera and the size of the detectors, as well as the presence of axial slat collimation). Both list-mode datasets were thus binned into 90 angles with single-slice rebinning (SSRB). SSRB is the simplest and most standard method for handling events in which 1 photon is detected in 1 transaxial slice and the corresponding photon is detected in another slice. SSRB simply places the event in the transaxial slice that bisects the 2 detected locations. The binned data were then corrected for “rotational weights” (11) and decay, multiplicatively corrected for attenuation effects, reconstructed with 8 iterations of ordered-subset expectation maximization (10 subsets), and postfiltered with a 3-dimensional Metz filter. No random or dead-time corrections were performed. The uniformity of the left ventricular wall distribution was assessed by calculating the SD of values from a maximum count circumferential profile program. Evaluation of contrast was made from manually drawn regions on the blood pool (BP) and the tissue of the left ventricle (LV) in a midventricular slice. The BP region comprised 4 voxels, and the LV region comprised 10 voxels. Reconstructed voxels for all phantom and patient studies were 0.47 cm on each side. Contrast was then calculated as $(\text{LV} - \text{BP})/(\text{LV} + \text{BP})$.

A ^{22}Na point source in air was also imaged with the axial slat collimators and with the LEHR collimators to measure resolution. The projections were binned and reconstructed in the same manner as the phantom data.

Patient Study. A patient with a prior myocardial infarction was given an oral glucose load, and a transmission scan was acquired. Three external markers (IZI Medical Products Corp., Baltimore, MD) filled with ^{99m}Tc were affixed to the patient, and a brief SPECT scan was obtained to help register the scans. The LEHR collimators used with the transmission scan were then changed to axial slat collimators, and FDG was added to the markers. The patient then received a 255-MBq (6.9 mCi) injection of FDG. Imaging was started 55 min later (181 MBq [4.9 mCi] FDG at scan start) with axial slat collimators. The collimators were then changed to the LEHR type, and the patient was imaged a second time, starting 133 min after injection (111 MBq [3.0 mCi] FDG at scan start). Both scans acquired data at 30 gantry angles for 60 s at each angle. The list-mode data were processed and reconstructed as described for the phantom data. The emission datasets were registered with the attenuation map by shifting to visually align the markers using an overlay display. Short-axis and polar maps were created from the attenuation-uncorrected and -corrected reconstructed transaxial slices. The same measure of LV-to-BP contrast as described for the phantom study was used for the patient data. The BP region comprised 9 voxels from midventricular slices, and the LV region comprised 20 voxels from a normally appearing region of heart tissue.

The Effect of ^{99m}Tc on Coincidence Imaging

A total of 156 MBq (4.2 mCi) ^{99m}Tc was added to the ^{18}F -loaded phantom to give a 7:1 $^{99m}\text{Tc}/^{18}\text{F}$ overall ratio at the time of imaging. Specifically, 10.3 MBq (0.28 mCi) ^{99m}Tc was added to the LV; a 3-cm³ defect with ^{18}F present was left without ^{99m}Tc . Seventy megabecquerels (1.9 mCi) were added to the liver, and 75.5 MBq (2 mCi) ^{99m}Tc were added to the background. With LEHR collimators in place, the phantom was imaged over 60 gantry angles for 30 s at each angle. Sensitivity (total number of photopeak–photopeak coincidences) and image quality were compared with and without the ^{99m}Tc present.

The Effect of FDG on ^{99m}Tc SPECT Imaging

The same phantom loaded with ^{18}F and ^{99m}Tc was imaged with SPECT with a 15% energy window centered at 140 keV. At the start of imaging, the $^{99m}\text{Tc}/^{18}\text{F}$ ratio was 9:1 (3.5:1 ratio in the heart). A 3.2:1 ratio in the heart has been reported to be the minimum expected when a dose of 925 MBq (25 mCi) ^{99m}Tc -sestamibi and 370 MBq (10 mCi) FDG is used (3,6). Because much less ^{18}F is sufficient with hybrid PET systems, this is a worst-case scenario. The acquisition was over 60 gantry angles for 20 s at each angle. Ten hours later, a ^{99m}Tc -alone scan with a $^{99m}\text{Tc}/^{18}\text{F}$ overall ratio of 138:1 was obtained with 60 gantry angles and 60 s at each angle. All SPECT phantom datasets were reconstructed with ordered-subset expectation maximization using attenuation compensation and depth-dependent point response compensation.

Crosstalk Correction for ^{99m}Tc SPECT Imaging

A multiple–energy window method was evaluated for crosstalk correction. The method assumes that the crosstalk from ^{18}F into the ^{99m}Tc photopeak window ($p_{140}(s, t, \phi)$, where s and t denote the coordinates in a 2-dimensional projection image at angle ϕ) can be approximated as a weighted average of smoothed data from energy windows adjacent to the 140-keV photopeak:

$$p_{140}(s, t, \phi) = k_u(p_{upper} \otimes g(\sigma_u))(s, t, \phi) + k_l(p_{lower} \otimes g(\sigma_l))(s, t, \phi), \quad \text{Eq. 1}$$

where \otimes indicates convolution, $g()$ is a 2-dimensional gaussian function $g(\sigma) = \frac{1}{2\pi\sigma^2} e^{(-s^2-t^2)/2\sigma^2}$, and k_u and k_l are scaling factors. A similar method has been used for estimating the crosstalk in the ^{201}Tl energy window when both ^{201}Tl and $^{99\text{m}}\text{Tc}$ are present (12).

The parameters k_u , σ_u , k_l , and σ_l were determined from a separate thorax phantom experiment. In this experiment, the phantom had only ^{18}F present but was imaged with SPECT with energy windows at 124 keV (7%), 140 keV (15%), and 162 keV (7%) to give p_{lower} , p_{140} , and p_{upper} . The 4 unknown parameters were estimated by minimizing:

$$\sum_{s,t,\phi} \|p_{140}(s, t, \phi) - p_{\text{est}}(s, t, \phi)\|, \quad \text{Eq. 2}$$

where

$$p_{\text{est}}(s, t, \phi) = k_u(p_{\text{upper}} \otimes g(\sigma_u))(s, t, \phi) - k_l(p_{\text{lower}} \otimes g(\sigma_l))(s, t, \phi). \quad \text{Eq. 3}$$

A nonlinear optimization routine (MATLAB; The MathWorks, Inc., Natick, MA) constrained to give parameters in the range 0.1–10.0 was used.

The crosstalk correction was tested by imaging a healthy volunteer. A resting $^{99\text{m}}\text{Tc}$ -sestamibi study was performed first (68 angles over 204° , 17 min total time). SPECT data were acquired 50 min after the injection of 955 MBq (25.8 mCi) $^{99\text{m}}\text{Tc}$ -sestamibi. Then, 159 MBq (4.3 mCi) FDG were injected, and the SPECT scan was repeated 84 min later so that at scan start there was a $^{99\text{m}}\text{Tc}/^{18}\text{F}$ whole-body ratio of 7.3:1. The energy windows were the same as those used for the ^{18}F phantom study. The SPECT data were reconstructed after the scaled smoothed crosstalk estimates (from Eq. 2 and the parameters from the phantom study) were subtracted from the projection data. Reconstruction was also performed by adding the crosstalk estimate to the projections at each iteration. The crosstalk correction schemes were evaluated by a noise measure (percentage root-mean-square error in a region of interest) and by a contrast measure ($[\text{LV} - \text{BP}]/[\text{LV} + \text{BP}]$). The BP region comprised 12 voxels over 2 midventricular slices, and the LV region comprised 8 voxels from a normally appearing region of heart tissue. The reconstructions were filtered with a 3-dimensional Metz filter for display.

RESULTS

Effect of LEHR Collimators on Coincidence Imaging

Phantom Study. Figure 1 compares ^{18}F phantom data imaged with axial slat collimators and with LEHR collimators. After scaling for decay and acquisition time, 36% more events were acquired with the LEHR collimators than with the axial slat collimators. The measure of uniformity of the activity distribution in the heart wall indicated that the wall was slightly less uniform when LEHR collimators were used (0.10 vs. 0.11) and much less uniform when attenuation correction was not performed (0.22). Contrast was better with axial slat collimators (0.98—the BP region was close to zero) than with LEHR collimators (0.80). The LEHR data did appear with distortions, which are addressed in the Discussion.

The in-plane resolution of the scanner in coincidence mode was 5.8 mm full width at half maximum both with axial slat collimators and with LEHR collimators. The axial resolution was 9.3 mm at the center of the field of view when axial slat collimators were used. With LEHR collimators, the axial resolution increased to 13.4 mm. Away from the center, axial resolution degraded with either collimator, but a much greater impact was seen for LEHR collimators.

Patient Study. The results from FDG imaging of the patient with axial slat and LEHR collimators are shown in Figure 2. Contrast was similar for the LEHR collimator images (0.45) and for the axial slat collimator images (0.47). Reduced contrast was expected from increased scatter in the LEHR images, but this increase might have been offset by additional clearing of the FDG from the BP and by FDG accumulation in tissues during the time between the 2 scans. Some extraneous activity was also apparent in the LEHR images.

Effect of $^{99\text{m}}\text{Tc}$ on Coincidence Imaging

With the 7:1 $^{99\text{m}}\text{Tc}/^{18}\text{F}$ overall ratio used in the phantom, little change in coincidence imaging was noted. After scaling for scan time and decay, the total number of coincidence

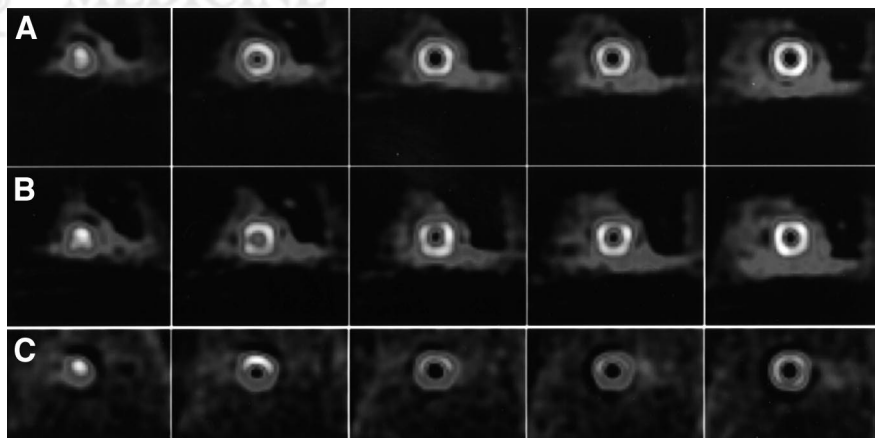


FIGURE 1. ^{18}F -only short-axis images of cardiac thorax phantom obtained with axial slat collimators (uniformity, 0.10) (A), LEHR collimators (uniformity, 0.11) (B), and axial slat collimators but without attenuation correction (uniformity, 0.22) (C). Short-axis slices appear somewhat square in (B); this anisotropic resolution effect is detailed in Discussion.

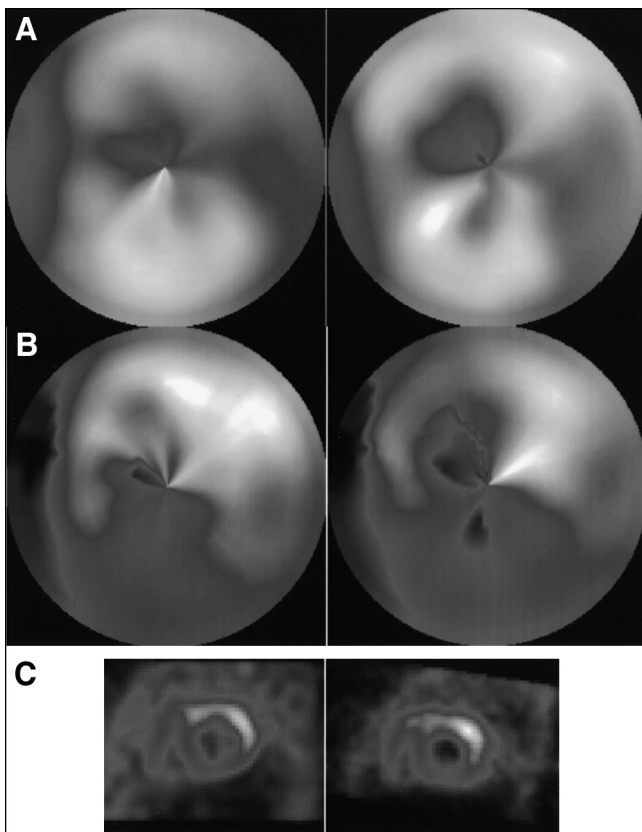


FIGURE 2. Patient data shown by polar maps with attenuation correction (A), polar maps without attenuation correction (B), and short-axis slices without attenuation correction (C). For all images, left side is with axial slat collimators and right side is with LEHR collimators.

events recorded changed $<5\%$, from 11.7 million without ^{99m}Tc present to 12.2 million with ^{99m}Tc present. Image quality was comparable between the 2 image sets, as seen in Figure 3.

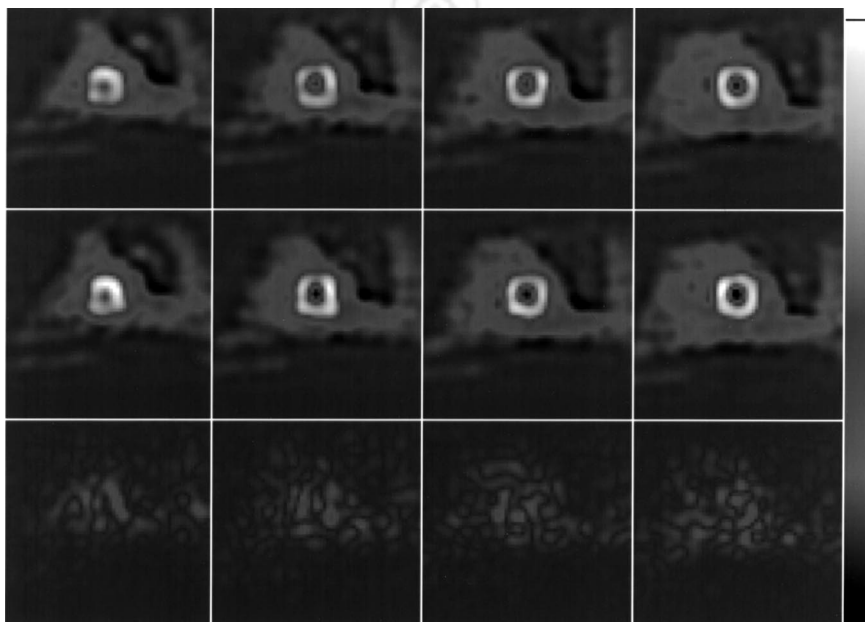


FIGURE 3. Four noncontiguous short-axis slices of phantom. Top row shows ^{18}F -only images obtained with LEHR collimators. Middle row shows images with ^{99m}Tc also present ($^{99m}\text{Tc}/^{18}\text{F}$ overall ratio, 7:1). Bottom row shows difference images.

Effect of FDG on SPECT Imaging

Figure 4 shows the SPECT reconstruction of the thorax phantom with ^{99m}Tc and ^{18}F present. Severe artifacts are obvious because of crosstalk from the ^{18}F . Approximately half the single photons detected in the ^{99m}Tc photopeak window were from ^{18}F crosstalk. The ^{99m}Tc -only image is also shown. The true defect can be seen in the ^{99m}Tc -only image, and artifactual defects appear from ^{18}F crosstalk.

The ^{18}F -only phantom study to estimate the crosstalk correction parameters is shown in Figure 5. The windows adjacent to the ^{99m}Tc photopeak appear similar to the photopeak data. Subtraction of the estimated crosstalk data in the photopeak gives a noisy residual centered on zero (Fig. 5B). The volunteer study shows that the transaxial slices are improved visually with crosstalk correction (Fig. 6), although the correction fails to remove the artifactual inferolateral defect. With respect to noise and contrast measures, Table 1 shows that contrast is improved with crosstalk correction but at the cost of at least some increase in noise.

DISCUSSION

When investigating the feasibility of imaging coincidence events and single photons together using LEHR collimators mounted on a hybrid PET system, one must consider 3 major issues. The first regards the use of standard LEHR collimators for FDG coincidence imaging. Significant degradations to the images were expected because, as in 3-dimensional PET, a much larger scatter fraction is obtained than when slat collimators are used. Watson et al. (13) have reported that, for thorax imaging with 3-dimensional PET, $>50\%$ of detected coincidences have undergone scattering in the object, compared with

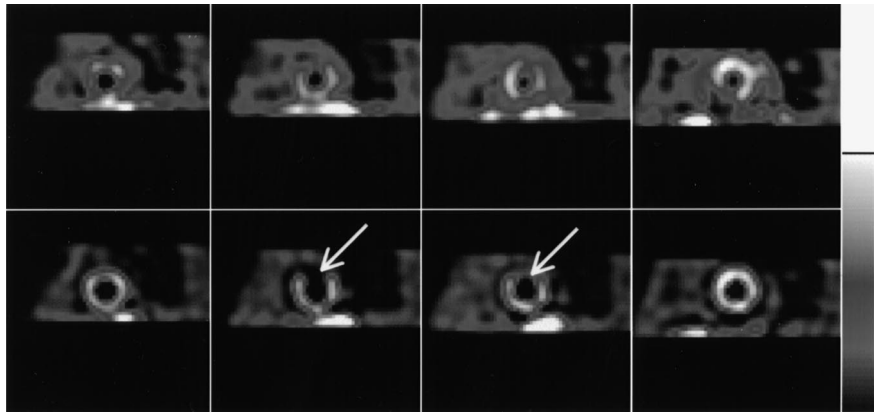


FIGURE 4. Phantom study for crosstalk levels. Top row shows images with ^{99m}Tc and ^{18}F present ($^{99m}\text{Tc}/^{18}\text{F}$ overall ratio, 9:1) and LEHR collimators. Bottom row shows ^{99m}Tc -only images ($^{99m}\text{Tc}/^{18}\text{F}$ overall ratio, 138:1). Arrows are pointing to true ^{99m}Tc defect.

10%–15% in 2-dimensional imaging. In the studies performed here, contrast was indeed reduced for the thorax phantom. However, the patient study revealed similar contrast with axial slat and LEHR collimators, possibly

because of increased physiologic contrast at the later imaging time of the LEHR scan.

Also important to consider is the large axial field of view of hybrid PET systems. When the thorax phantom with only FDG was imaged in coincidence mode with LEHR collimators, significant image distortions were evident when SSRB was used; axially oblique acceptance angles were not limited by collimation or by software. The distortions produce short-axis slices that appear somewhat square, likely because of the poor axial resolution inherent with SSRB. Thus, a cylinder with the long axis perpendicular to the z -axis of the scanner would appear somewhat square because the resolution is not isotropic. That is, the cylinder walls parallel to the z -axis will be blurred more than will the walls perpendicular to the z -axis. With axial slat collimators or with PET systems having a small axial extent, the oblique angles are likely small enough for the effect to be negligible. Others have shown squared-off (as in Figs. 1 and 3) phantom results with hybrid PET (5), though no comment was made. As a test of this anisotropic resolution hypothesis, the list-mode coincidence data were reconstructed with a fully 3-dimensional algorithm (3-dimensional tilt angle binning (14,15)) that provides more uniform spatial resolution than does SSRB. The myocardial short-axis slices became less square, as seen in Figure 7. Although the LEHR data did result in degraded images, even the SSRB images appeared to retain much of the clinical value (Fig. 2).

Although seemingly not an issue for the patient study shown here, activity outside the field of view may be a significant problem with LEHR collimators. Placing extra shields of lead on the ends or covering portions of the patient with curved lead slabs may improve the data by blocking these photons. This problem is found with 3-dimensional PET systems as well (16,17).

The second issue that was investigated was the effect of the presence of ^{99m}Tc while imaging FDG. This issue was found not to be critical when a threshold detector was used to discard events less than approximately 200 keV and when relatively low counting rates were used. Serious performance trade-offs are to be expected with other scenarios.

The third issue was to determine the degree of crosstalk into the ^{99m}Tc energy window and to test a simple correction

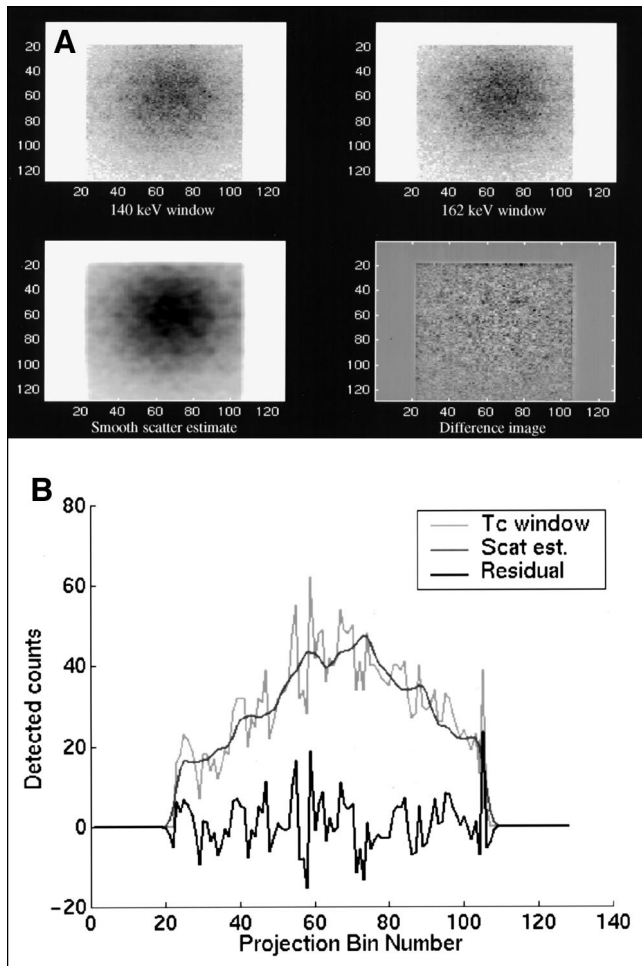


FIGURE 5. Phantom study for crosstalk compensation. (A) Reverse grayscale images. Top left shows ^{99m}Tc window. Top right shows 162-keV window. Bottom left shows smooth scatter estimate (from Eq. 1). Bottom right shows difference or residual between ^{99m}Tc window and smooth scatter estimate. (B) Horizontal profile through row 27 of images in A (162-keV window profile not shown). Scat est. = smooth scatter estimate.

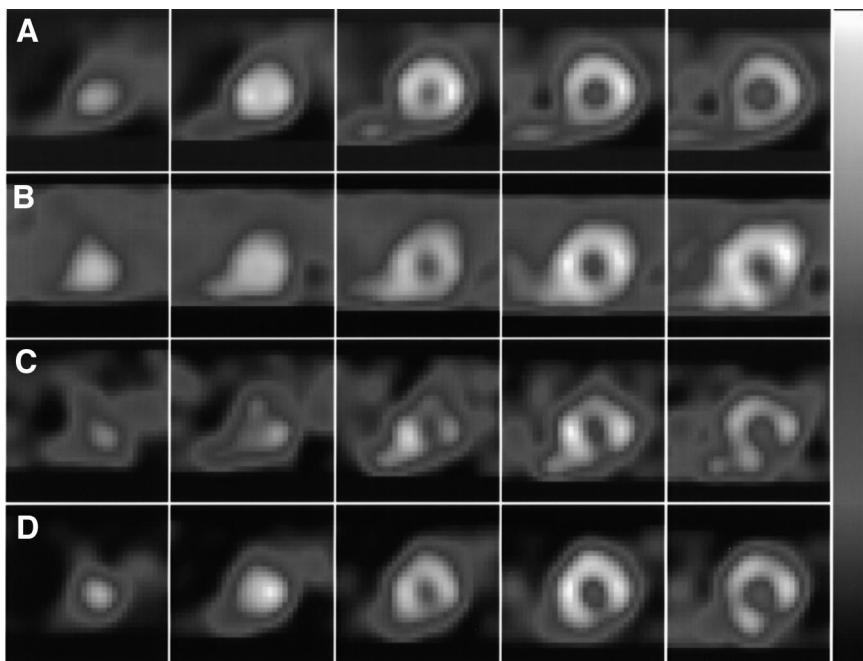


FIGURE 6. Reconstructions from SPECT imaging of volunteer with only sestamibi present (A), with sestamibi and FDG present and crosstalk compensation (B), with sestamibi and FDG present and subtraction of crosstalk estimate (C), and with sestamibi and FDG present and inclusion of crosstalk estimate in iterative reconstruction algorithm (D). Even with correction, artifactual inferolateral defect remains.

scheme. Compared with dual-isotope imaging with 511-keV collimators, the situation is dramatically different with LEHR collimators. The scatter contribution has little structure because the collimator has little effect on the 511-keV photons. One group has found encouraging results after compensating for crosstalk (18,19). In 1 study (19), the group used a triple-energy window scatter subtraction technique with $^{18}\text{F}/^{99\text{m}}\text{Tc}$ in a brain phantom with a hybrid PET system. Their method is equivalent to using Equation 1 without any smoothing and letting $k_l = k_u = 1.5$ and using 5% wide energy windows on either side of the 140-keV photopeak.

On the basis of our finding that approximately half the single photons detected in the $^{99\text{m}}\text{Tc}$ photopeak window were from ^{18}F crosstalk, we determined that the 3.2:1 $^{99\text{m}}\text{Tc}/^{18}\text{F}$ ratio in the heart reported as useful for dual-isotope 511-keV SPECT is not high enough to perform dual-isotope coincidence/single-photon imaging. In addition, ^{18}F not only adversely affects the imaging of $^{99\text{m}}\text{Tc}$ by crosstalk in the $^{99\text{m}}\text{Tc}$ photopeak, but the large number of ^{18}F photons causing scintillations not in the $^{99\text{m}}\text{Tc}$ photopeak may affect the dead time of the camera so that fewer $^{99\text{m}}\text{Tc}$ photons are detected. A vital question, which was not addressed in this

study, is how little FDG can be used without degrading clinical FDG viability images. A clinical report in which 19 women received simultaneous injections of $^{99\text{m}}\text{Tc}$ -sestamibi and FDG at stress (740 MBq [20 mCi] $^{99\text{m}}\text{Tc}$ and 74 MBq [2 mCi] ^{18}F initially) and were imaged 50 min later with PET and then 4–6 h later with SPECT shows that minimizing the crosstalk from ^{18}F may make such imaging possible (20,21). It should be noted that a standard SPECT camera with a thin crystal and therefore reduced crosstalk was used for imaging of $^{99\text{m}}\text{Tc}$ -sestamibi (20).

The crosstalk compensation method used here improved the images, but artifacts remained. As with the phantom images in Figure 4, using a similar $^{99\text{m}}\text{Tc}/^{18}\text{F}$ ratio, artifactual defects result from the crosstalk of FDG. An alternative to Equation 1, using instead a very smooth version of the 511-keV coincidence projections (after binning with SSRB), was investigated both by itself and in conjunction with Equation 1. These alternative formulations did not match the measured p_{140} data as well. More sophisticated crosstalk compensation methods and the presence of less FDG should provide better results.

TABLE 1
Comparison of Reconstruction Methods

Method	Contrast	% RMS error
With no crosstalk compensation	0.23	57
With crosstalk model presubtracted	0.32	87
With crosstalk model in reconstruction	0.28	64

RMS = root-mean-square.

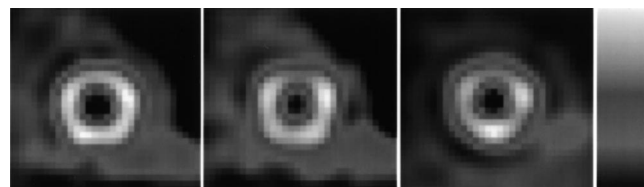


FIGURE 7. Comparison of reconstruction using 3-dimensional tilt angle binning and SSRB for ^{18}F data acquired with LEHR collimators. Left image was obtained with axial slat collimators; middle image, with LEHR collimators and SSRB; and right image, with LEHR collimators and 3-dimensional tilt angle binning.

The advantage of sequential $^{99m}\text{Tc}/^{18}\text{F}$ imaging with LEHR collimators is primarily that the data are likely to be registered, which can be important when assessing perfusion and glucose uptake matches and mismatches. As well, only a single transmission scan is needed to correct both sets of data. Throughput also increases relative to a sequential axial slat/LEHR collimator protocol because the collimators do not need to be changed. Imaging may not be possible with axial slat collimators and large amounts of ^{99m}Tc present because the hybrid PET systems have a poor counting-rate performance and the high number of ^{99m}Tc single photons may cause significant dead time. Finally, successful sequential imaging implies that truly simultaneous imaging will be possible.

CONCLUSION

If feasible, imaging ^{18}F and ^{99m}Tc together with coincidence/single-photon imaging is an exciting way to extend the usefulness of the new hybrid PET systems. The results imply that with high $^{99m}\text{Tc}/^{18}\text{F}$ whole-body ratios ($>9:1$), low FDG doses, and state-of-the-art reconstruction and crosstalk correction, performing immediately sequential coincidence/single-photon imaging with clinically useful results will likely be practical. Simultaneous coincidence/SPECT imaging may also be possible, although the counting-rate capability of the camera when both coincidence and single photons must be processed is of critical importance.

ACKNOWLEDGMENTS

This study was supported by a grant from the Whitaker Foundation. Portions of this study were presented at the annual meeting of the Society of Nuclear Medicine, Los Angeles, CA, 1999, and at the midwinter meeting of the Society of Nuclear Medicine, New Orleans, LA, 2000.

REFERENCES

- Chen EQ, MacIntyre WJ, Go RT, et al. Myocardial viability studies using fluorine-18-FDG SPECT: a comparison with fluorine-18-FDG PET. *J Nucl Med.* 1997;38:582-586.
- Srinivasan G, Kitsiou AN, Bacharach SL, et al. [^{18}F]fluorodeoxyglucose single photon emission computed tomography: can it replace PET and thallium SPECT for the assessment of myocardial viability? *Circulation.* 1998;97:843-850.
- Sandler MP, Bax JJ, Patton JA, et al. Fluorine-18-fluorodeoxyglucose cardiac imaging using a modified scintillation camera. *J Nucl Med.* 1998;39:2035-2043.
- Patton JA, Turkington TG. Coincidence imaging with a dual-head scintillation camera. *J Nucl Med.* 1999;40:432-441.
- Fukuchi K, Sago M, Nitta K, et al. Attenuation correction for cardiac dual-head γ camera coincidence imaging using segmented myocardial perfusion SPECT. *J Nucl Med.* 2000;41:919-925.
- Sandler MP, Videlefsky S, Delbeke D, et al. Evaluation of myocardial ischemia using a rest metabolism/stress perfusion protocol with fluorine-18 deoxyglucose/technetium-99m MIBI and dual isotope simultaneous-acquisition single-photon emission computed tomography. *J Am Coll Cardiol.* 1995;26:870-878.
- Delbeke D, Videlefsky S, Patton JA, et al. Rest myocardial perfusion/metabolism imaging using simultaneous dual-isotope acquisition SPECT with technetium-99m-MIBI/fluorine-18-FDG. *J Nucl Med.* 1995;36:2110-2119.
- Stoll H-P, Hellwig N, Alexander C, et al. Myocardial metabolic imaging by means of fluorine-18 deoxyglucose/technetium-99m sestamibi dual-isotope single-photon emission tomography. *Eur J Nucl Med.* 1994;21:1085-1093.
- Sandler MP, Patton JA. Fluorine 18-labeled fluorodeoxyglucose myocardial single-photon emission computed tomography: an alternative for determining myocardial viability. *J Nucl Cardiol.* 1996;3:342-349.
- Zubal IG, Daley L, Ng C, et al. Coincidence and collimated emission tomography acquired on a dual headed camera system [abstract]. *J Nucl Med.* 1998;39(suppl):132P.
- Clack R, Townsend D, Jeavons A. Increased sensitivity and field of view for a rotating positron camera. *Phys Med Biol.* 1984;29:1421-1431.
- Moore SC, English RJ, Syravanh C, et al. Simultaneous Tc-99m/Tl-201 imaging using energy-based estimation of the spatial distribution of contaminant photons. *IEEE Trans Nucl Sci.* 1995;42:1189-1195.
- Watson CC, Newport D, Casey ME, et al. Evaluation of simulation-based scatter correction for 3D PET cardiac imaging. *IEEE Trans Nucl Sci.* 1997;44:90-97.
- Kadmas DJ, Di Bella EVR, Gullberg GT. An alternative binning method and iterative OSEM algorithm for fully 3D volume-of-interest reconstruction. Paper presented at: International Meeting on Fully Three-Dimensional Image Reconstruction in Radiology and Nuclear Medicine; June 23-26, 1999; Egmond aan Zee, The Netherlands.
- Kadmas DJ, Di Bella EVR, Chapman BE, et al. 3D tilt angle binning (3D-TAB): description and comparison with FORE, FORE-J, and SSRB [abstract]. *J Nucl Med.* 2000;41(suppl):133P.
- Bailey DL, Miller MP, Spinks TJ, et al. Experience with fully 3D PET and implications for future high resolution 3D tomographs. *Phys Med Biol.* 1998;43:777-786.
- Spinks TJ, Miller MP, Bailey DL, et al. The effect of activity outside the direct field of view in a 3D-only whole-body positron tomograph. *Phys Med Biol.* 1998;43:895-904.
- Baron JM, Zubal IG, Daley L, et al. Simultaneous coincidence and Tc99m SPECT imaging using a dual purpose camera with collimators and a cross-talk correction algorithm [abstract]. *J Nucl Med.* 1999;40(suppl):119P.
- Zubal IG, Narayanan MV, MacMullan J, et al. Scatter correction for camera based coincidence and single photon imaging protocols. *IEEE Trans Nucl Sci.* 2000;47:1222-1227.
- Abramson BL, Ruddy TD, deKemp RA, et al. Stress perfusion/metabolism imaging: a pilot study for a potential new approach to the diagnosis of coronary disease in women. *J Nucl Cardiol.* 2000;7:205-212.
- Jain D, McNulty PH. Exercise-induced myocardial ischemia: can this be imaged with F-18-fluorodeoxyglucose? [editorial]. *J Nucl Cardiol.* 2000;7:286-288.